RMetS

Royal Meteorological Society

Downscaling of monthly precipitation using CMIP5 climate models operated under RCPs

Umut Okkan[a],* and Umut Kirdemir[b]
[a] *Department of Civil Engineering, Balikesir University, Turkey*
[b] *Department of Civil Engineering, Izmir Institute of Technology, Turkey*

ABSTRACT: Downscaling of general circulation model (GCM) outputs extracted from CMIP5 datasets to monthly precipitation for the Gediz Basin, Turkey, under Representative Concentration Pathways (RCPs) was performed by statistical downscaling models, multi-GCM ensemble and bias correction. The output databases from 12 GCMs were used for the projections. To determine explanatory predictor variables, the correlation analysis was applied between precipitation observed at 39 meteorological stations located over the Basin and potential predictors of ERA-Interim reanalysis data. After setting both artificial neural networks and least-squares support vector machine-based statistical downscaling models calibrated with determined predictor variables, downscaling models producing the most suitable results were chosen for each meteorological station. The selected downscaling model structure for each station was then operated with historical and future scenarios RCP4.5, RCP6.0 and RCP8.5. Afterwards, the monthly precipitation forecasts were obtained from a multi-GCM ensemble based on Bayesian model averaging and bias correction applications. The statistical significance of the foreseen changes for the future period 2015–2050 was investigated using Student's *t* test. The projected decrease trend in precipitation is significant for the RCP8.5 scenario, whereas it is less significant for the RCP4.5 and RCP6.0 scenarios.

KEY WORDS   statistical precipitation downscaling; CMIP5 data; RCPs; ERA-Interim reanalysis data; multi-GCM ensemble; correcting bias

Received 23 November 2015; Revised 10 February 2016; Accepted 19 February 2016

1. Introduction

General circulation models (GCMs) can be taken into consideration to obtain climate change projections for hydro-meteorological variables. In spite of their practical usage, the main problem with the projections produced from GCMs is their coarse resolution. Therefore, downscaling strategies have been developed (Wilby and Wigley, 1997).

In the literature, downscaling methods have been classified into two groups: dynamical and statistical downscaling (Wilby *et al.*, 1998). Dynamical downscaling is related to regional climate modelling. Simulating local climate characteristics can be feasible using dynamical models (Leung *et al.*, 2003), yet they have several drawbacks in terms of their demanding design and computational redundancy (Fowler *et al.*, 2007).

Statistical downscaling methods are used to transform the outputs from GCMs to the local scale by means of mathematical relationships derived from different methods (Okkan and Inan, 2015a). These kinds of methods require less computational effort than dynamical downscaling applications and are considered to be the most practical downscaling techniques in the hydro-meteorology literature (Tripathi *et al.*, 2006). Regression-based techniques (e.g. Wilby *et al.*, 1998; Hessami *et al.*, 2008), weather generator (Semenov, 2008) and artificial neural networks can be preferred. Successful downscaling studies carried out with artificial neural networks (ANNs) under different climate change scenarios can be found in the literature

(Goyal and Ojha, 2012; Okkan and Fistikoglu, 2014; Okkan, 2015; Okkan and Inan, 2015b).

In spite of the many superiorities of ANNs, they also have drawbacks, including the local minima problem and complexity in determining layered architecture (Suykens, 2001). Support vector machines (SVMs) and two-parameter version called least-squares support vector machines (LSSVMs) can be considered as alternatives to ANNs without their disadvantages. SVMs and LSSVMs have shown remarkable results in statistical downscaling content. In a study carried out by Tripathi *et al.* (2006), an LSSVM was applied to future forecasts from the CGCM2 to obtain future projections of monthly precipitation for the meteorological sub-divisions in India. Similar methods were applied by Anandhi *et al.* (2008) to downscale precipitation to a study region in Karnataka State, India. A statistical downscaling strategy based upon a modified SVM model was developed by Chen *et al.* (2010) to forecast precipitation in a basin in China. Sachindra *et al.* (2013) employed an LSSVM for transforming GCM simulations to local scale flows observed in northwestern Victoria, Australia.

Many of downscaling studies mentioned above have considered previous climate change scenarios, which are mentioned in the Intergovernmental Panel on Climate Change (IPCC)-Fourth Assessment Report (AR4) as the Special Report on Emission Scenarios (SRES). However, the Fifth Assessment Report (AR5) of the IPCC published in 2014 provided new scenarios termed 'Representative Concentration Pathways' (RCPs). RCPs comprise groups of several scenarios that produce emission pathways related to the future emissions of greenhouse gases, aerosols, ozone and land use/land cover changes, whereas AR4 scenarios (SRES) included only forcing by greenhouse gases and aerosols (Moss *et al.*, 2010; Meinshausen *et al.*, 2011).

* Correspondence: U. Okkan, Department of Civil Engineering, Hydraulic Division, Balikesir University, 10145, Balikesir, Turkey. E-mail: umutokkan@balikesir.edu.tr
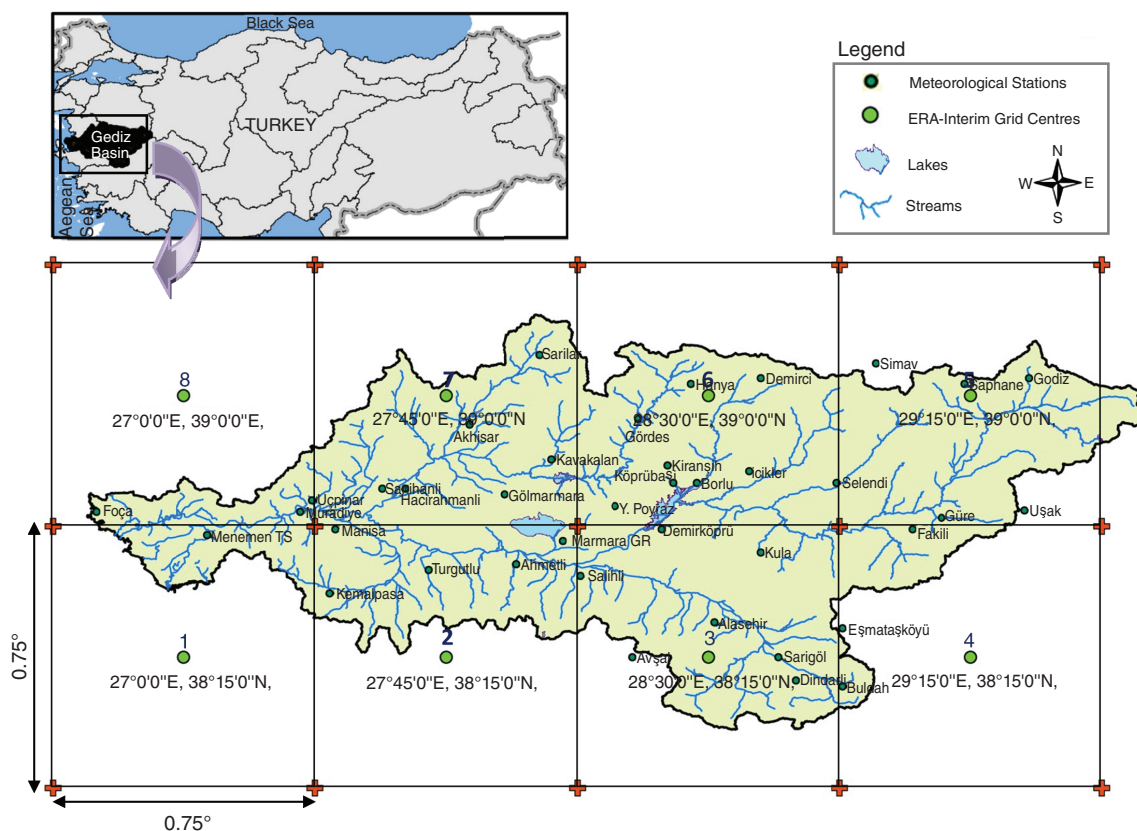
Figure 1. Location of Gediz Basin (Turkey), meteorological stations within the Basin and ERA-Interim grid coverage.

These emission pathways are classified with the radiative forcing generated by the end of the 21st Century. In this context, Coupled Model Inter-comparison Project Phase 5 (CMIP5) services datasets of new-generation GCMs under different RCPs.

More recently, several studies in the literature have adopted RCP scenarios to assess possible climatic change effects on hydrological variables. In a study presented by Chong-hai and Ying (2012), alteration in air temperature and precipitation over regions located in China were described based on the outputs of various GCMs with projections of 21st century climate under different RCP scenarios. Kim *et al.* (2013) examined the separated and combined effects of probable changes in climate and land use/land cover on streamflow for the Hoeya Basin, South Korea, using two RCP scenarios. Ji and Kang (2013) used a dynamical downscaling model with two RCP scenarios to project precipitation and temperature over the Tibetan Plateau. Lee *et al.* (2014) presented another dynamical downscaling work about the evaluation of future climate change over East Asia considering two RCPs. Analysis of precipitation lapse rate over north Sikkim, eastern Himalayas, under RCPs was also performed by Singh and Goyal (2016).

The present study explores the potential of statistical downscaling methods, evaluates the downscaled multiple GCMs with an ensemble approach and uses new scenarios for projecting monthly precipitation over Gediz Basin in the Aegean region of Turkey. The explanatory predictor selection work is investigated prior to outlining the downscaling process. The potential predictor selection was provided from the monthly ERA-Interim reanalysis dataset. The calibrated and validated downscaling model structure was integrated to 12 GCMs with three RCP scenarios. The precipitation forecasts were obtained from multi-GCM ensemble through a Bayesian model averaging method followed by correcting biases. The bias-corrected forecasts produced for the near future period (2015–2050) were then examined to understand the probable climate change impacts on the precipitation regime.

To the best of our knowledge, a statistical downscaling study concerning the use of RCP scenarios for climate projections in Turkey has not been realized previously. Projected changes of hydrometeorological variables for different basins in Turkey under SRES of AR4 have been obtained from the simulation of GCMs in version three of the Coupled Model Inter-comparison Project, CMIP3 (e.g. Okkan and Fistikoglu, 2014; Okkan and Inan, 2015a, 2015b) However, in the present work, projections derived from statistical downscaling techniques are introduced based on CMIP5 data in the hope of providing a reference for investigating the probable climatic change impacts on the precipitation regime in the Basin under different RCPs.

The paper is structured in four sections. The properties of the study region, the reanalysis and GCM data, selection of the predictor and statistical downscaling techniques are presented in the next section. The results obtained are given in the third section, and the summary and conclusions form the concluding part of the paper.

2. Data and methodology

2.1. Study region and preparing data

The application area covers the Gediz Basin in Turkey, which is located in the Aegean Region (Figure 1). The Gediz River is the second-largest river in Turkey flowing into the Aegean Sea. The total drainage area of the Basin is 17 125 km^2. The Basin is bordered by mountains and hills to the north, south and east.

Table 1. Meteorological stations in the Gediz Basin, Turkey, where observed precipitation data were used for the downscaling exercise.

Station name	Station number	MGM/DSI	Altitude (m)	Latitude (°) N	Longitude (°) E
Akhisar	17184	MGM	93	38.917	27.817
Ahmetli	5617	MGM	100	38.517	27.950
Alaşehir	5974	MGM	189	38.350	28.517
Borlu	2425	MGM	250	38.750	28.467
Demirci	17746	MGM	851	39.050	28.650
Foça	5434	MGM	10	38.667	26.750
Gediz	17750	MGM	825	39.050	29.417
Gölmarmara	5273	MGM	150	38.717	27.917
Gördes	4930	MGM	550	38.933	28.300
Güre	5458	MGM	650	38.650	29.167
Köprübaşı	5278	MGM	250	38.750	28.400
Kula	5624	MGM	675	38.550	28.650
Manisa	17186	MGM	71	38.617	27.433
Menemen TS	9020	MGM	10	38.600	27.067
Muradiye	5440	MGM	25	38.667	27.333
Salihli	17792	MGM	111	38.483	28.133
Şaphane	4765	MGM	925	39.033	29.233
Sarıgöl	6143	MGM	225	38.250	28.700
Saruhanlı	5269	MGM	50	38.733	27.567
Selendi	5282	MGM	575	38.750	28.867
Turgutlu	5615	MGM	120	38.500	27.700
Avşar	05-026	DSI	275	38.250	28.283
Buldan	05-027	DSI	470	38.167	28.883
Demirköprü	05-003	DSI	290	38.617	28.367
Dindarlı	05-006	DSI	685	38.183	28.750
Eşm ataşköyü	05-001	DSI	930	38.333	28.883
Fakılı	05-012	DSI	715	38.617	29.083
Hacırahmanlı	05-002	DSI	45	38.733	27.633
Hanya	05-010	DSI	640	39.033	28.450
İcikler	05-018	DSI	710	38.783	28.617
Kavakalan	05-011	DSI	460	38.817	28.050
Kıranşıh	05-016	DSI	670	38.800	28.383
Marmara GR	05-023	DSI	75	38.583	28.083
Sarılar	05-008	DSI	340	39.117	28.017
Üçpınar	05-007	DSI	100	38.700	27.367
Y. Poyraz	05-013	DSI	630	38.683	28.233
Uşak	17188	MGM	919	38.671	29.404
Simav	17748	MGM	809	39.093	28.979
Kemalpaşa	5785	MGM	200	38.433	27.417

Turkish State Meteorological Service (MGM); General Directorate of State Hydraulic Works (DSI).

The region includes broad irrigation plains with an area of nearly 110 000 ha where intensive agricultural practices are carried out. Grape, maize, cotton and various other fruits and vegetables are the main crops grown in the Basin. A major part of existing water resources is used for irrigation purposes because agriculture is the major economic activity in the region. The Demirkopru Dam located in the centre of the Basin has the largest reservoir and Marmara Lake is the other main water supply for irrigation. The other dams in the Basin have relatively small reservoirs.

The monthly precipitation data measured at the Basin were obtained from 39 meteorological stations for the period January 1980 to December 2005. The study area has a Mediterranean climate. The average temperature in summer in the basin varies from 23.5 to 25.5 °C, that of winter varies from 5.3 to 6.8 °C, and the mean annual temperature is 15 °C. The majority of measured rainfall is observed in the winter, whereas summer is much drier. The total annual areal precipitation calculated from the Thiessen polygon method is about 550 mm for the same period. In recent years, like many basins with Mediterranean climate characteristics, the Gediz Basin has suffered from water scarcity because of drought resulting from decreased precipitation, increased temperature and rapid demographic development. Thus, projecting precipitation under different climate change scenarios is important for water resource planning in this region of Turkey.

The observed monthly precipitation records at 39 meteorological stations located in the Gediz Basin (Figure 1; station numbers and their geographical coordinates are given in Table 1) were used for the statistical downscaling exercise. The station records were provided from the Turkish State Meteorological Service (MGM) and General Directorate of State Hydraulic Works (DSI). Monthly precipitation data of each station from January 1980 to December 2005 were considered as the predictand, whereas ERA-Interim monthly reanalysis data from the European Centre for Medium-Range Weather Forecasts (ECMWF) were selected as potential predictor variables for the observation period.

ERA-Interim reanalysis data have been used frequently as possible predictors for downscaling in the literature (Bürger et al., 2012; Haas and Pinto, 2012; Vu et al., 2015). The variables of the determined eight ERA-Interim grids (Figure 1) covering the basin, with latitudes 37.875–39.375 ° N and longitudes

Table 2. Information about selected general circulatin models (GCMs).

GCM name	Institution	Modelling centre	Resolution Latitude (°) × Longitude (°)	Centre coordinates of used grids which cover the study area
BCC-CSM1	Beijing Climate Center, China Meteorological Administration, China	BCC	1.121 × 1.125	[38.69 ° N, 27 ° E]; [38.69 ° N, 28.125 ° E]; [38.69 ° N, 29.25 ° E]
CCSM4	National Center for Atmospheric Research, USA	NCAR	0.942 × 1.25	[38.17 ° N, 27.5 ° E]; [38.17 ° N, 28.75 ° E]; [39.11 ° N, 28.75 ° E]; [39.11 ° N, 27.5 ° E]
CESM1(CAM5)	National Center for Atmospheric Research, USA	NCAR	0.942 × 1.25	[38.17 ° N, 27.5 ° E]; [38.17 ° N, 28.75 ° E]; [39.11 ° N, 28.75 ° E]; [39.11 ° N, 27.5 ° E]
CSIRO-Mk3.6	Commonwealth Scientific and Industrial Research Organisation, Australia	CSIRO-QCCCE	1.865 × 1.875	[38.24 ° N, 26.25 ° E]; [38.24 ° N, 28.125 ° E]; [38.24 ° N, 30 ° E]
GFDL-CM3	Geophysical Fluid Dynamics Laboratory, USA	NOAA GFDL	2 × 2.5	[39 ° N, 26.25 ° E]; [39 ° N, 28.75 ° E]
GFDL-ESM2M	Geophysical Fluid Dynamics Laboratory, USA	NOAA GFDL	2.022 × 2.5	[37.416 ° N, 26.25 ° E]; [37.416 ° N, 28.75 ° E]; [39.438 ° N, 28.75 ° E]; [39.438 ° N, 26.25 ° E]
GISS-E2-H	NASA Goddard Institute for Space Studies, USA	NASA GISS	2 × 2.5	[39 °N, 26.25 °E]; [39 °N, 28.75 °E]
GISS-E2-R	NASA Goddard Institute for Space Studies, USA	NASA GISS	2 × 2.5	[39 ° N, 26.25 ° E]; [39 ° N, 28.75 ° E]
HadGEM2-ES	Met Office Hadley Centre, UK	MOHC	1.25 × 1.875	[38.75 ° N, 26.25 ° E]; [38.75 ° N, 28.125 ° E]; [38.75 ° N, 30 ° E]
IPSL-CM5A-LR	Institut Pierre-Simon Laplace, France	IPSL	1.895 × 3.75	[38.842 ° N, 26.25 ° E]; [38.842 ° N, 30 ° E]
MIROC-ESM	Atmosphere and Ocean Research Institute, Japan	MIROC	2.791 × 2.813	[37.673 °N, 28.125 °E]
MRI-CGCM3	Meteorological Research Institute, Japan	MRI	1.12 × 1.125	[38.69 ° N, 27 ° E]; [38.69 ° N, 28.125 ° E]; [38.69 ° N, 29.25 ° E]

26.625–29.625 °E, were compiled from the ECMWF website http://apps.ecmwf.int/datasets/. Each grid presented in Figure 1 has a spatial resolution of 0.75°. Thus, a box covering the basin was obtained at a resolution of 1.5° × 3.0°.

The large-scale output databases from 12 GCMs, which include both historical scenario outputs representing past climates and future climate simulations under the RCP4.5, RCP6.0, and RCP8.5 scenarios, were selected for the downscaling exercise in the Basin under RCP scenarios. Another scenario, RCP 2.6, which is the most optimistic scenario in terms of CO_2 emissions, was not examined in this study because hydrometeorological tendencies observed in the Basin point out probable warming and water scarcity problems that could occur in the near future. In the present study, the 1980–2005 period was used for historical scenario simulations, whereas the 2015–2050 period was considered for RCP simulations. The selected RCPs represent different radiative forcing pathways from greenhouse gas emissions resulting from anthropogenic actions, with radiative forcing of 4.5, 6.0 and 8.5 W m^{-2} by 2100, respectively. For the year 2100, the greenhouse gas concentrations for RCP4.5, RCP6.0, and RCP8.5 are equivalent to 650, 850 and >1370 parts *per* million CO_2, respectively. Compared to other RCPs, RCP8.5 corresponds to the pathway with the maximal greenhouse gas emission. It is assumed that excessive population and slow income growth with modest rates of technological change will be effective under RCP8.5 scenario (Riahi *et al.*, 2011).

The CMIP5 set of experiments shares RCP simulations of various GCMs through several gateway websites operated by the Earth System Grid Federation (ESGF). In the study, the large-scale scenario outputs, which comprise both historical climate and future simulations forced by RCPs, were extracted from the gateway website http://pcmdi9.llnl.gov/esgf-web-fe/. Information about selected GCMs and the centre co ordinates of the grids covering the study region are given in Table 2.

In this study, 11 ERA-Interim variables, which were common to data involved in 12 GCMs having 3 RCP scenarios, were extracted with the intention of establishing statistical downscaling models based on ANN/LSSVM techniques to transform GCM outputs to the monthly precipitation for 39 meteorological stations. The dataset consists of several variables including mean air temperature (air), geo-potential height (hgt) and relative humidity (rhum) at different atmospheric levels (200, 500 and 850 hPa), large-scale precipitation (pr) and sea-level pressure (slp) at Earth's surface, which are the probable predictor variables. An interpolation procedure was also used to get the outputs of GCMs at reanalysis grid box consisting of eight ERA-Interim grids because the grid centers of employed GCMs may not be consistent with reanalysis grid center.

2.2. Predictor selection

In the statistical downscaling literature, exercises confirm that explanatory predictors can change from one location to another. Any predictor can be considered before the downscaling step, but only if it shows plausible correlation with the observations (Fistikoglu and Okkan, 2011). Determining the predictors through correlation–regression analyses is frequently preferred (Hessami *et al.*, 2008; Fistikoglu and Okkan, 2011), although the relationships between some variables can be nonlinear and selecting the predictors via linear regression-based techniques may not seem true at first sight. Wilby *et al.* (2002) also advised a predictor selection procedure through regression analysis within the context of some guidelines for scenario usage. There are

Table 3. Summary of All Possible Regression method (APREG) analyses for Manisa station.

Number of variables in the best subsets	C_p	RMSE (mm)	air850	hgt850	rhum850	air500	hgt500	rhum500	air200	hgt200	air	slp	pr
1	9.7	28.35											√
2	8.1	28.23					√						√
3	7.3	28.15									√	√	√
4	4.3	27.97	√	√							√		√
5	2.2	27.83	√				√	√			√		√
6	3.7	27.85	√				√	√		√	√		√
7	4.3	27.83	√			√		√		√	√	√	√
8	6.1	27.87	√	√		√		√		√	√	√	√
9	8	27.91	√	√	√	√		√		√	√	√	√
10	10	27.95	√	√	√	√		√	√	√	√	√	√
11	12	28.00	√	√	√	√	√	√	√	√	√	√	√

Air, mean air temperature (°C); slp, sea level pressure (hPa); pr, large-scale precipitation (kg m^{-2}); hgt, geo-potential height (m); rhum, relative humidity (%). 200, 500, and 850 near the variables denote the related atmospheric level (hPa).

various ways of determining predictors, too. The All Possible Regression method (APREG), which was also used in this study context, is another effective tool to determine the best subset of predictors (Fistikoglu and Okkan, 2011). In APREG application assessment of subset regression combinations can be based on conventional measurements such as the root mean squared error (RMSE) and Mallows' C_p co-efficient. Details about the APREG procedure applied to downscaling studies were given by Fistikoglu and Okkan (2011) and Okkan and Fistikoglu (2014).

In the APREG application for this study, the monthly precipitation values observed at 39 meteorological stations located in the basin were the predictand variables, whereas variables in the ERA-Interim reanalysis were the probable predictor data. The predictors are composed of the average of the values belonging to eight grids enclosing the basin. As a representative example, a summary of the results obtained from the APREG for Manisa station is given in Table 3. According to Table 3, Mallows' C_p co-efficient decreases rapidly up to five-regressor model and then increases with the use of further variables. It can be said also that the large-scale *pr* variable of the reanalysis dataset, which appeared in all input combination as a predictor, increased the statistical relationship, confirming what other studies in the literature have emphasized previously (Salathé, 2003; Tatli *et al.*, 2004; Xoplaki *et al.*, 2004; Schmidli *et al.*, 2006).

The common belief is that the subset regression model with the lowest RMSE and C_p should be chosen as the best one. However, performances of *k*-regressor models having *k* predictor are nearly the same as that of the one-regressor model including only the *pr* variable; that is, the RMSE values calculated from one-regressor and *k*-regressor models are nearly equal for all stations. In other words, it can be observed that the change in RMSE is no longer meaningful when the number of predictors exceeds one (Figure 2). Thus, the predictor selection process determined the model with one variable as optimum, which implies that only large-scale *pr* is sufficient for the downscaling of monthly precipitation over the whole Basin.

2.3. ANN and LSSVM

One of the downscaling models used in this study is based on artificial neural networks (ANNs). ANNs can be defined as a black box technique producing output against input(s) and is one of the preferred statistical downscaling techniques. Among various algorithms applied to a typical ANN structure composed of feed forward and back propagation steps, a second-order optimization

algorithm called the Levenberg–Marquardt algorithm (LM) is quite successful because it is generally faster and more suitable than other algorithms. Hagan and Menhaj (1994) presented a comprehensive description of ANNs with LM.

The Support Vector Machine (SVM) is another artificial intelligence algorithm constructed with statistical learning theory. Despite successful modelling performance of SVM, it has several disadvantages which were discussed in Suykens (2001). However, the least squares support vector machine (LSSVM) shows a computational benefit over the conventional support vector machine method by transforming the quadratic optimization experience into a linear equation system. Tripathi *et al.* (2006) presented a detailed description of the LSSVM applied to downscaling modelling.

2.4. Performance metrics for ANN/LSSVM models

Moriasi *et al.* (2007) indicated the significance of the use of three metrics, namely, Nash–Sutcliffe efficiency (NS), root mean squared error-observations standard deviation ratio (RSR) and bias percentage (PBIAS), to examine predicting capabilities. These metrics were also employed in this study for comparing two statistical downscaling models, although originally they were intended for hydrological model assessment. The formulations of these metrics and ratings pertaining to metrics were given by Moriasi *et al.* (2007).

3. Results

3.1. Training and testing of statistical downscaling models

First, and before starting the downscaling modelling, all data were divided into two periods for application: the training period (January 1980 to December 1992) and the testing period (January 1993 to December 2005). The downscaling strategy proposed in this study was designed with a MATLAB code and summarized in Figure 3. In this study, all data were standardized before being input into two statistical models because z-score standardization makes the training of a downscaling model capable. This standardization procedure also was applied to scenario data of GCMs as mentioned in Figure 3.

In the training period of the ANN/LSSVM using reanalysis data, estimation of optimal values for the related parameters were important. In the training of the ANN with the LM algorithm, the numbers of neurons in the hidden layer (n.n.h) made RMSE
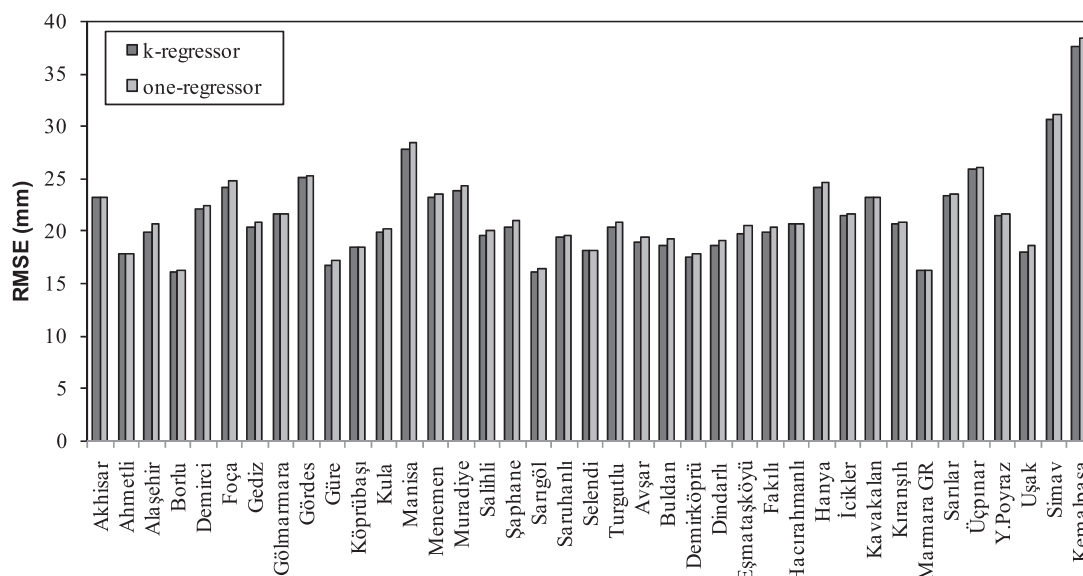
Figure 2. RMSE statistics calculated from *k*-regressor and one-regressor models.

statistics the lowest were determined iteratively (Table 4). The parameters of the LM algorithm, which are the initial Marquardt parameter (μ_0) and decay rate (β), were selected as 0.010 and 0.1, respectively. In addition, by monitoring the relative changes on RMSE statistics, the optimal epoch number could be chosen after several trials operated in the MATLAB-ANN toolbox.

The LSSVM model needs the calibration of two parameters: the regularization parameter (γ) and the Gaussian radial basis function (GRBF) width (σ). In the LSSVM training period, the grid-search method under *k*-fold cross-validation was applied to estimate optimal LSSVM parameters (see Table 4), which made RMSE the lowest in the training. After different trials for this study, the number of folds was selected as 10. The grid search method can yield an optimal parameter set and employing a cross-validation procedure can prevent the downscaling model from over-fitting. The authors refer readers to a MATLAB tool-box available at http://www.esat.kuleuven.ac.be/sista/lssvmlab.

After the training period of the ANN- and LSSVM-based statistical downscaling models, the performances of two models were assessed by means of NS, RSR and PBIAS. Determination co-efficient R^2 values also were computed to interpret the amount of explained variance. In the study, only testing period performances were introduced because both the ANN and LSSVM showed similar capabilities in terms of performance metrics during the training period. Table 4 shows performance indices of models for the testing period (January 1993 to December 2005) to compare their generalization capabilities. As a representative example, time-series plots and scatter plots of monthly precipitation predictions at Akhisar station are presented in Figure 4, both for the training and testing periods.

The results of the ANN model show that NS co-efficients in the basin range from 0.57 to 0.84 during the testing period. Although the RSR efficiencies for the ANN model in the basin vary from 0.39 to 0.66, the computed PBIAS statistics are between 9.5 and −20.5%. The PBIAS performances of the ANN model for 36 stations are considered as 'very good'. Moreover, stations modelled with ANN show 'good' and 'very good' performances in terms of RSR and NS, except for five stations. On the other hand, NS and RSR measures computed from the LSSVM are nearly the same as those of the ANN model. In this sense, the LSSVM also provides 'good' and 'very good' modelling performances

except for two stations (Fakilli and Ucpinar stations), whereas the PBIAS values for the LSSVM point out 'very good' performance at 36 stations. The performance ratings are available at Moriasi *et al.* (2007).

During the training and testing of the models, both the ANN and LSSVM gave quite similar results in terms of the performance indices. Although the two models produced satisfactory results in general, it turned out that slightly better results were obtained with some stations using one of the models rather than the other. According to overall performance criteria during the testing period for each station, it was decided which downscaling model would be used in the stage of downscaling GCM outputs to station scale (see last column in Table 4).

Although the results achieved from the two models showed a good/very good consistency in precipitation predictions at nearly all stations, the capability for extreme value estimation of employed models was found to be restricted at some stations. In the literature, it has been emphasized that this scenario is quite possible because the statistical models may not explain the entire variance of the modelled predictand (Tripathi *et al.*, 2006).

3.2. Downscaling outputs of 12 GCMs to precipitation and multi-GCM ensemble application

In the previous section, a convenient statistical downscaling model that had a better performance than the other one was sought in order to downscale reliably the raw RCP outputs of used GCMs to precipitation at 39 stations. After the model construction for each station, values of *pr* for individual grids were arranged for the GCMs of the historical scenario and for RCP4.5, RCP6.0, and RCP8.5 future scenarios. According to the downscaling scheme introduced in Figure 3, after preparing interpolated data for each GCM, which are a combination of the values of the nearest grids covering the Gediz Basin (given in the last column of Table 2) and those of neighbouring grids, the RCP datasets were standardized with the historical scenario statistics of the corresponding GCM. These standardized series were considered as the input vector for the selected statistical downscaling models calibrated through the reanalysis variables compiled from eight ERA-Interim grids. Thus, for each GCM, standardized values representing the historical and future scenarios were made
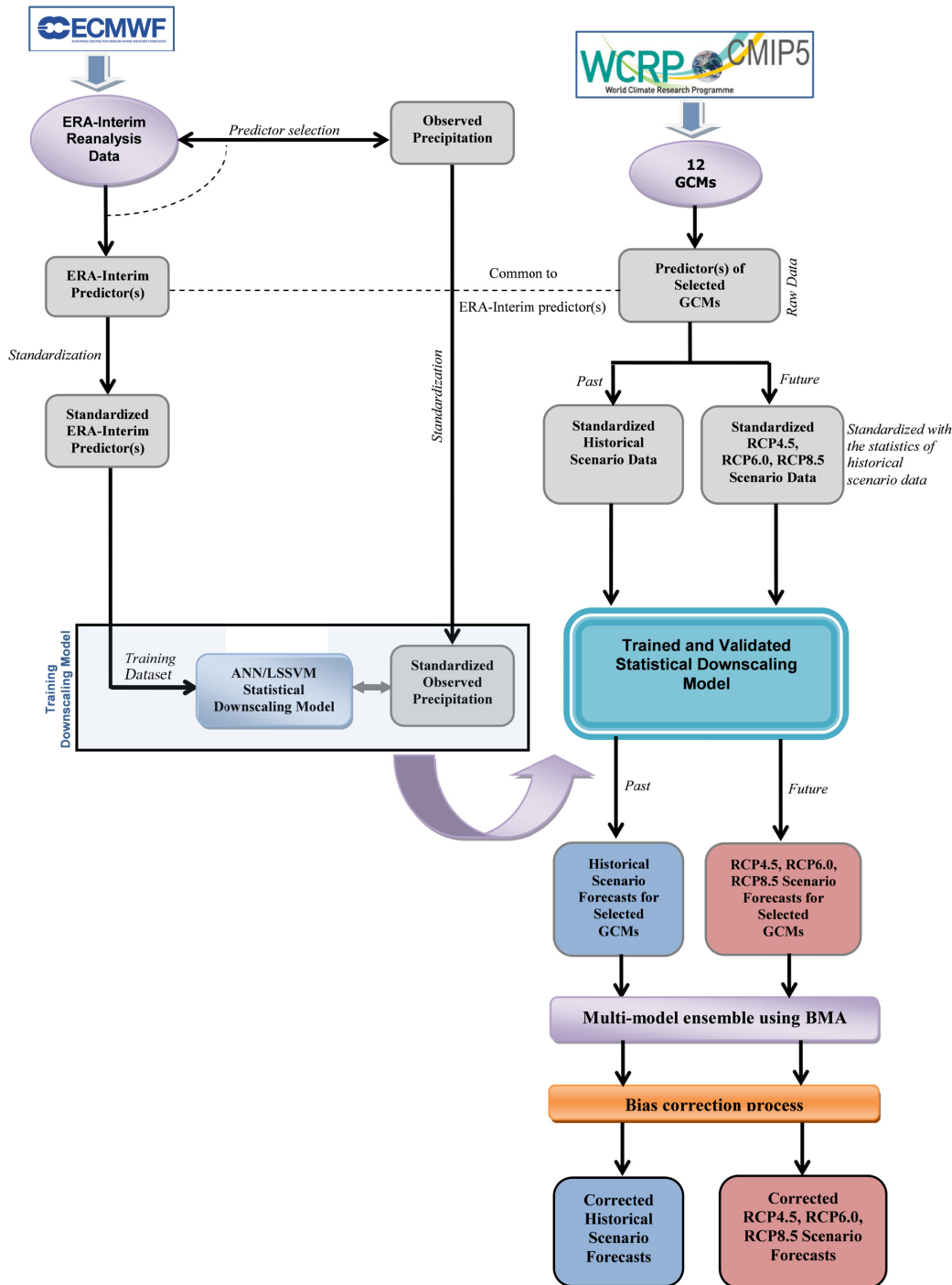
Figure 3. Proposed downscaling strategy applied in the study.

for all meteorological stations. Following the simulation process by trained downscaling model, the obtained standardized values were turned into precipitation unit (in millimetre).

The statistically downscaled precipitation series of 12 GCMs at meteorological station scales were inspected through the box plot graphs under different scenarios. It was seen from the graphs that some descriptive statistics, especially the medians, interquartile ranges and upper whiskers in RCPs, varied relatively from one GCM to another (Figure 5 (a)–(d) for an example at Simav station).

In the literature, there are several inspirational studies focusing on the uncertainties originating from the differences between

forecasts obtained from different GCMs (Dibike *et al.*, 2007; Mujumdar and Ghosh, 2008; Okkan and Inan, 2015a). It is apparent that no single GCM is superior to other GCMs for all kinds of downscaling work and under all climatic circumstances. In this respect, the multi-GCM ensemble procedure operating with a group of comparable GCM simulations has been suggested by some researchers to deliver more accurate projections (Knutti *et al.*, 2010; Chong-hai and Ying, 2012; Okkan and Inan, 2015a). An ensemble strategy used in hydrological modelling studies may also help to improve the uncertainty estimation (Duan *et al.*, 2007). A comprehensive review on multi-GCM ensemble applications in the literature and some frequently used

Table 4. Overall performance measures of the artificial neural network (ANN) and least-squares support vector machine (LSSVM) statistical downscaling models for the testing period.

Stations	ANN					LSSVM						Selected
	n.n.h	R^2	NS	RSR	PBIAS (%)	γ	σ	R^2	NS	RSR	PBIAS (%)	Downscaling model
Akhisar	5	0.7775	0.7762	0.4715	3.68	5.64E+01	0.43	0.7756	0.7742	0.4736	3.60	ANN
Ahmetli	4	0.7561	0.7354	0.5128	0.30	1.69E+03	31.78	0.7471	0.7365	0.5117	0.47	LSSVM
Alaşehir	6	0.6657	0.6620	0.5795	3.03	5.90E+00	0.42	0.6593	0.6530	0.5871	1.25	ANN
Borlu	3	0.7750	0.7461	0.5022	−4.94	9.68E+00	0.37	0.7749	0.7472	0.5012	−5.50	LSSVM
Demirci	13	0.7838	0.7795	0.4681	−2.92	2.18E+04	0.89	0.7771	0.7722	0.4757	−3.55	ANN
Foça	3	0.7808	0.7795	0.4681	3.13	5.20E+07	57.56	0.7782	0.7773	0.4704	3.21	ANN
Gediz	6	0.7261	0.7256	0.5221	−1.32	7.35E+07	15.93	0.7217	0.7211	0.5264	−0.88	ANN
Gölmarmara	13	0.7635	0.7600	0.4883	3.07	2.02E+04	86.02	0.7605	0.7587	0.4896	2.12	ANN
Gördes	4	0.7541	0.7392	0.5091	0.83	2.84E+04	130.70	0.7610	0.7435	0.5048	−1.76	LSSVM
Güre	2	0.6696	0.6573	0.5835	−3.67	2.97E+04	117.04	0.6759	0.6738	0.5693	−1.70	LSSVM
Köprübaşı	5	0.7386	0.6868	0.5579	−14.42	1.62E+03	37.01	0.7488	0.6974	0.5483	−16.36	LSSVM
Kula	1	0.6655	0.6423	0.5962	−2.54	1.52E+04	29.65	0.6811	0.6677	0.5746	−1.83	LSSVM
Manisa	6	0.8417	0.8363	0.4033	−5.86	6.23E+05	1.14	0.8355	0.8332	0.4071	−5.19	ANN
Menemen	2	0.8108	0.8091	0.4355	−3.41	3.18E+02	1.53	0.8060	0.8044	0.4408	−3.69	ANN
Muradiye	4	0.8364	0.8351	0.4048	−2.49	6.53E+06	1.34	0.8417	0.8386	0.4005	−4.20	LSSVM
Salihli	6	0.7230	0.7183	0.5291	−0.66	7.70E+01	6.66	0.7155	0.7132	0.5338	−1.19	ANN
Şaphane	1	0.7056	0.6439	0.5948	−10.21	3.70E+05	270.45	0.7251	0.6756	0.5677	−7.04	LSSVM
Sarıgöl	3	0.6696	0.6599	0.5813	2.37	4.25E+05	75.52	0.6836	0.6786	0.5651	2.28	LSSVM
Saruhanlı	5	0.8372	0.8212	0.4214	−8.99	3.64E+04	29.10	0.8283	0.8154	0.4283	−9.79	ANN
Selendi	2	0.6463	0.6194	0.6149	3.05	4.74E+04	36.88	0.6800	0.6655	0.5765	1.59	LSSVM
Turgutlu	14	0.7926	0.7921	0.4545	−1.16	8.70E+01	0.81	0.7867	0.7865	0.4606	−0.88	ANN
Avşar	4	0.7080	0.7040	0.5423	5.25	3.41E+04	64.18	0.7052	0.6962	0.5494	5.03	ANN
Buldan	11	0.7316	0.7124	0.5346	−9.23	1.65E+06	304.03	0.7322	0.7277	0.5201	−5.50	LSSVM
Demirköprü	6	0.7713	0.7637	0.4846	−0.96	5.32E+04	158.26	0.7742	0.7701	0.4780	−0.44	LSSVM
Dindarlı	6	0.6947	0.6901	0.5549	4.24	1.26E+06	99.83	0.7016	0.6932	0.5522	4.30	LSSVM
Eşmetaşköyü	7	0.6865	0.6681	0.5743	8.41	5.29E+05	5.39	0.6701	0.6500	0.5897	8.13	ANN
Fakıllı	4	0.5814	0.5650	0.6575	9.59	9.61E+02	13.95	0.5809	0.5560	0.6642	10.02	ANN
Hacırahmanlı	8	0.7728	0.7727	0.4752	−1.04	3.60E+01	0.39	0.7752	0.7734	0.4745	−3.15	LSSVM
Hanya	4	0.7636	0.7390	0.5092	−3.83	1.28E+04	73.46	0.7718	0.7329	0.5151	−7.35	ANN
İcikler	1	0.6666	0.6600	0.5812	0.37	1.28E+05	50.64	0.6779	0.6682	0.5742	2.61	LSSVM
Kavakalan	11	0.8164	0.8114	0.4329	0.99	2.44E+03	35.13	0.8225	0.8130	0.4310	−2.64	LSSVM
Kıranşıh	8	0.7752	0.7505	0.4979	−4.03	1.78E+01	0.25	0.7740	0.7475	0.5009	−4.98	ANN
Marmara GR	4	0.7422	0.7356	0.5126	3.41	2.50E+03	43.68	0.7470	0.7447	0.5037	2.96	LSSVM
Sarılar	8	0.8255	0.8126	0.4315	−5.53	1.83E+04	0.99	0.8272	0.8142	0.4297	−6.00	LSSVM
Üçpınar	5	0.7085	0.6362	0.6012	−20.49	2.25E+06	27.94	0.7223	0.6366	0.6009	−22.18	LSSVM
Y.poyraz	12	0.7665	0.7464	0.5020	−4.86	6.40E+00	0.24	0.7537	0.7425	0.5058	−4.39	ANN
Uşak	6	0.7206	0.7199	0.5275	2.09	2.44E+01	0.46	0.7104	0.7095	0.5373	2.15	ANN
Simav	1	0.8024	0.7815	0.4660	−6.57	1.51E+03	27.90	0.8075	0.7857	0.4614	−6.97	LSSVM
Kemalpaşa	14	0.8474	0.8437	0.3941	−5.30	4.79E+06	1.28	0.8445	0.8402	0.3985	−6.25	ANN

The underlined values in table represent the optimal results.

methods was discussed at the 'IPCC Expert Meeting on Assessing and Combining Multi Model Climate Projections' by Knutti *et al.* (2010). Their work provided useful practical advice for using multi-GCM ensembles in climate projections which should be essential for impact-adaptation exercises. In this regard, criteria for modelling quality and performance indices, and weighting of employed models were discussed.

Concerning the recommendations of Knutti *et al.* (2010), the weighted multi-GCM mean approach was preferred, which is an average across all forecasts from multi-GCM simulations, that does not treat the used GCMs equally. In this approach, the weights can be derived from some measures assessing GCM capability in simulating the observed climate conditions (Knutti *et al.*, 2010). The ensemble procedure for this study was performed with the Bayesian Model Averaging (BMA) method. This is a statistical scheme designed to obtain probabilistic forecasts with greater ability and reliability than the forecasts obtained by any single model. In some studies, BMA was shown to yield convenient results when it was compared with other ensemble techniques (Raftery *et al.*, 2005). BMA has been used formerly in hydro-meteorological applications. For example, Raftery *et al.* (2005) used BMA in order to calibrate forecast ensembles in numerical weather modelling. To the best of our knowledge, a multi-GCM ensemble exercise focusing on the BMA scheme has not been found in the downscaling literature. The BMA method is given concisely as follows.

Consider a quantity y to be the modelled variable, $D = [y_{obs,1}, y_{obs,2}, \ldots, y_{obs,T}]$ to be the observed data with data size T, and f_k forecasts obtained from the K-model ($K = 12$ for this study), where the *a posteriori* distribution of y is represented as the conditional probability $p_k (y|f_k, D)$.

Referencing the total probability law, the probabilistic forecast of BMA is defined as the probability density function shown in Equation ((1):

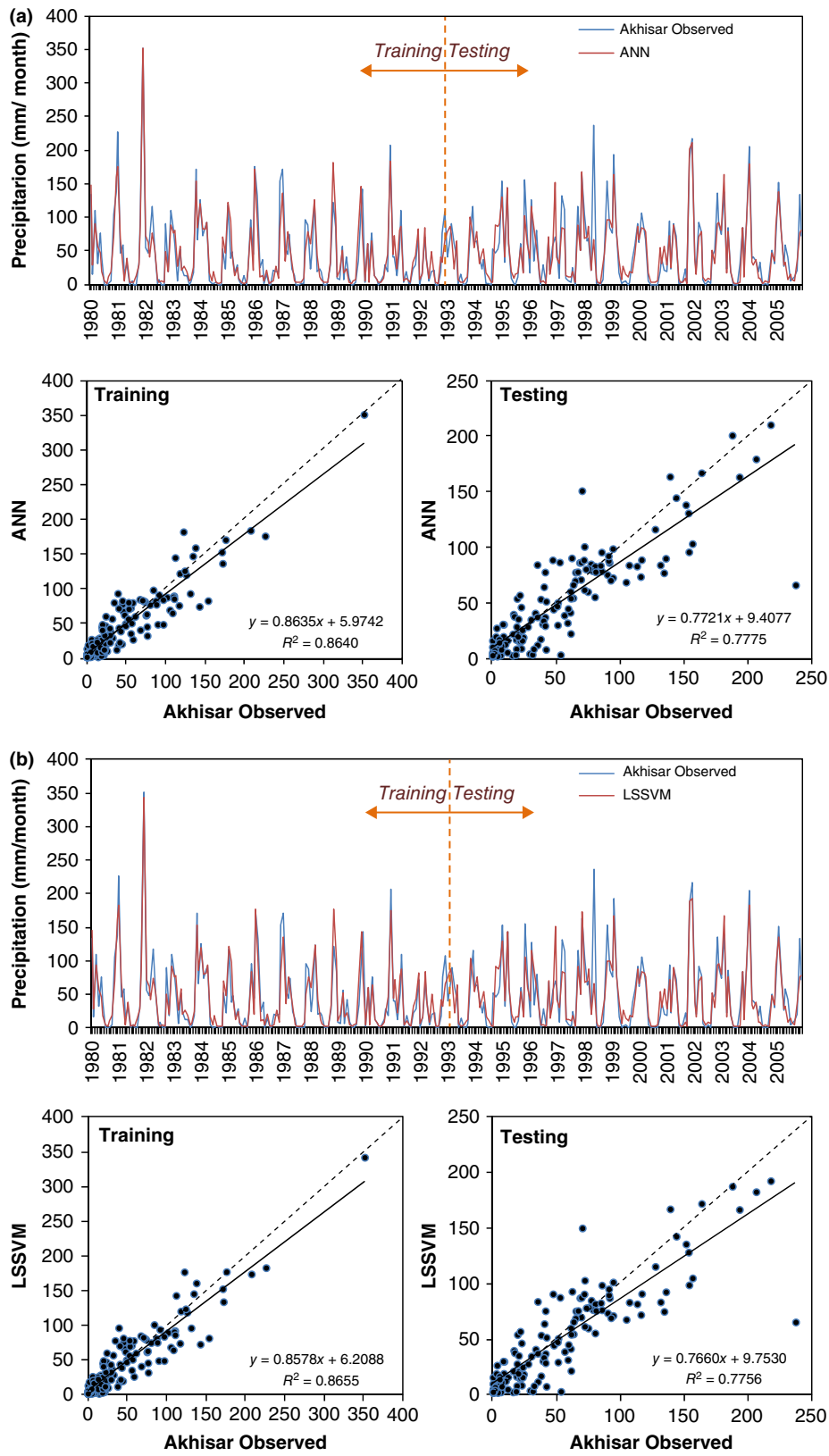$$p(y|D) = \sum_{k=1}^{K} p(f_k|D) \cdot p_k(y|f_k, D) \tag{1}$$

Figure 4. Precipitation predictions (in millimetre) derived from (a) ANN and (b) LSSVM for the historical period (1980–2005) at Akhisar station.
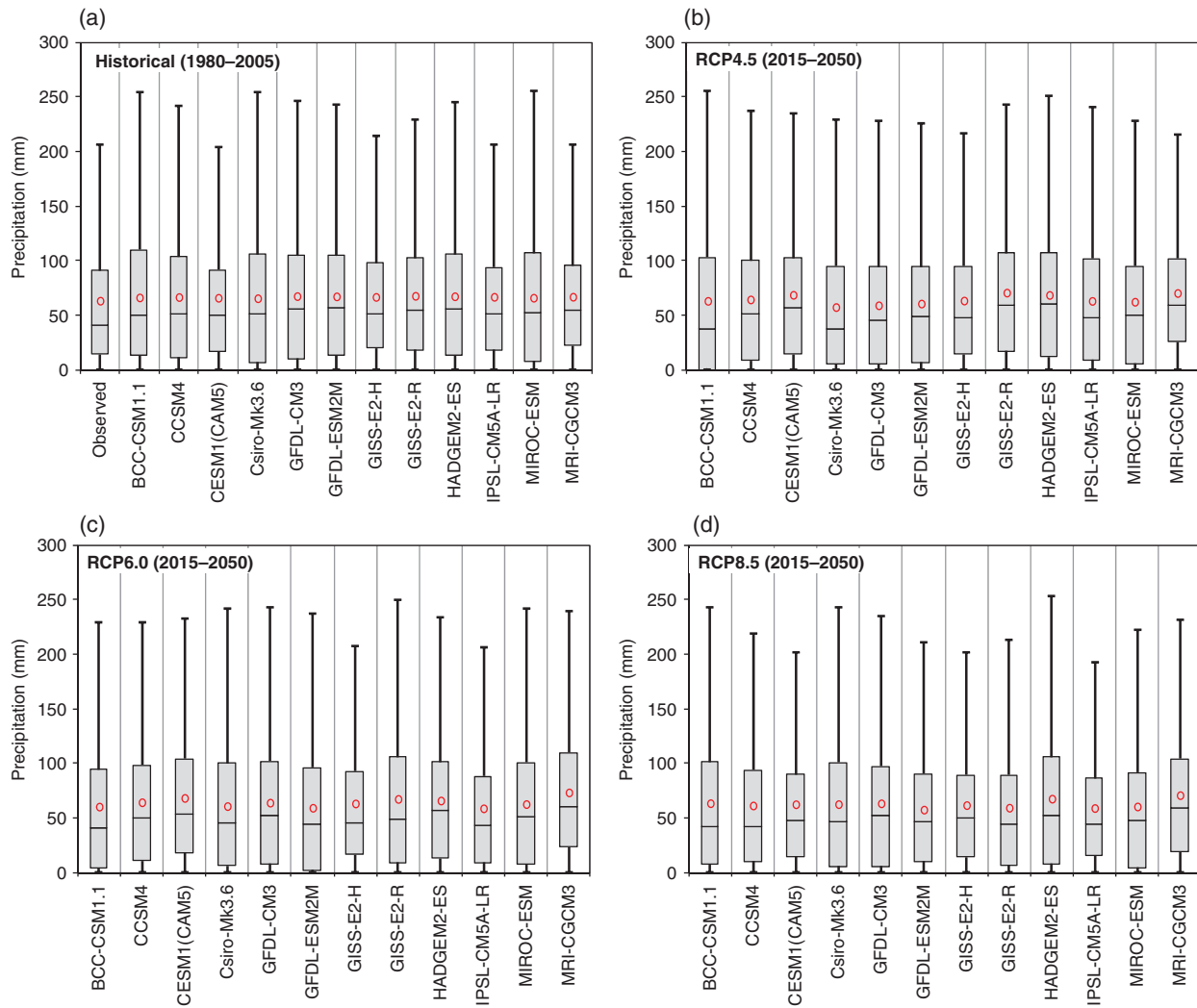
Figure 5. Scenario precipitation forecasts obtained from downscaled values of 12 GCMs at Simav station: (a) historical, (b) RCP4.5, (c) RCP6.0 and (d) RCP8.5.

This term also measures how well model forecasts match the observations. To gain a computational convenience in practice, Gaussian distribution is assumed for $p_k(y|f_k, D)$, which is also denoted as $g(y|f_k, \sigma_k^2)$. Assuming that the probability distribution of precipitation error is non-Gaussian, data are subjected to the Box–Cox transformation before applying BMA. If weights are defined as $w_k = p(f_k|D)$, then BMA gives $\Sigma w_k = 1$, where w_k are all positive. The posterior mean of the BMA forecast is defined as shown in Equation ((2):

$$E\left[y|D\right] = \sum_{k=1}^{K} p\left(f_k|D\right) \cdot E\left[p_k\left(y|f_k, D\right)\right]$$
$$= \sum_{k=1}^{K} w_k \cdot f_k \qquad (2)$$

To apply the BMA method, weights (w_k) and the variance of model forecast (σ_k^2) must be estimated. The maximization of a log-likelihood function (Equation ((3)) suggested by Raftery *et al.* (2005) can be used for this step:

$$l(\theta) = l\left(w_1, \ldots, w_k; \sigma_1, \ldots, \sigma_k\right) = \log[\sum_{k=1}^{K} w_k \cdot g\left(y|f_k, \sigma_k\right)]$$
$$(3)$$

However, obtaining an analytical solution of θ by conventional methods is quite difficult. For that reason, Raftery *et al.* (2005) has recommended an iterative procedure based on the Expectation–Maximization algorithm (E-M). For a detailed description of both the BMA scheme and E-M, readers are referred to Duan *et al.* (2007).

In order to apply the BMA method for precipitation projection, an ensemble of competing forecasts from 12 GCMs (historical scenario forecasts) was considered. In the study, precipitation forecasts were divided into two periods as wet (from October to March) and dry (from April to September) and then applied the BMA to each period separately. Thus, a different set of BMA weights was obtained for each period. The computed weights for 39 stations were not given due to space limitations. After computing weights for each station during the historical scenario period, downscaled values of 12 GCMs for 3 RCPs were multiplied by these weights and then summed to obtain future scenario results.

3.3. Bias correction

Some studies in the literature have revealed that the results derived from the multi-model mean approach generally outperform those from single GCMs compared to measured values

Mean (mm)	SD (mm)	C_v	Median (mm)
46.450	52.430	1.129	28.450
Min. (mm)	Max. (mm)	Skewness	Kurtosis
0.001	351.200	1.760	4.380

Mean (mm)	SD (mm)	C_v	Median (mm)
45.890	29.460	0.642	41.980
Min. (mm)	Max. (mm)	Skewness	Kurtosis
1.910	124.170	0.410	-0.710

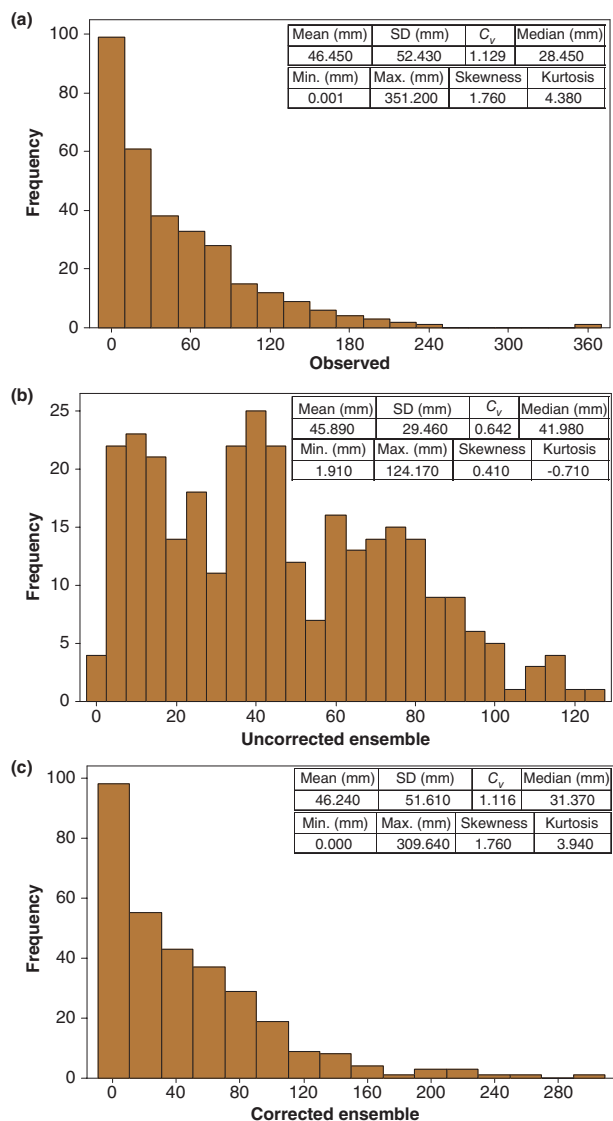| Mean (mm)	SD (mm)	C_v	Median (mm)
46.240	51.610	1.116	31.370
Min. (mm)	Max. (mm)	Skewness	Kurtosis
0.000	309.640	1.760	3.940

Figure 6. Histogram plots of (a) observed precipitation, (b) uncorrected ensemble forecasts under historical scenario and (c) corrected ensemble forecasts under historical scenario at Akhisar station.

(Gleckler *et al.*, 2008). However, some biases may be observed in ensemble simulations (Knutti *et al.*, 2010). In this section, following the ensemble process based on the BMA scheme given in the previous section, a bias correction technique was used so as to lessen possible biases in ensemble forecasts. It is possible that the forecasts produced from statistical downscaling models may contain some biases due to several reasons attributed to GCM resolution, the predictors, preferred downscaling model type and the climate period. Sachindra *et al.* (2014) have emphasized that correcting biases is required before use of projections in climate impact studies.

There are various bias correction methods applied to raw GCM outputs and also to the downscaled values. The most frequently used technique is quantile mapping (QM) that can be capable of correcting the statistical moments. In this method, cumulative distribution functions (CDFs) of downscaled past scenario results are mapped onto the CDFs of observations. For future climate scenarios, first, corresponding to the downscaled values for future periods, the CDFs are computed from the CDFs relating to the past scenario results. Finally, the corrected values of

a variable for future periods can be extracted from the CDFs of the observations (Sachindra *et al.*, 2014). Lafon *et al.* (2013) used linear-nonlinear scaling, Gamma distribution-based QM and empirical distribution-based QM (EMQM) in their work. According to their comparisons, EMQM was determined as the best-performing method. EMQM also displayed successful performance in a study presented by Themeßl *et al.* (2011). Ines and Hansen (2006) compared the performances of QM and the multiplicative shift method (MSF) in correcting the bias for precipitation values. They concluded that MSF corrected the long-term monthly mean precipitation. However, this method is unsuccessful for correcting systematic errors in precipitation distribution. Sachindra *et al.* (2014) presented a comprehensive study involving the usage of equidistant QM (EDQM), monthly bias-correction (MBC) and nested bias-correction (NBC) methods. When considering the performances of three methods, EDQM was preferred for preparing future precipitation projections in their work.

In this study, QM based bias correction strategy was applied. The approach employed, which was formulized by Ghosh and Mujumdar (2008), used CDFs to reduce the biases existing in scenario forecasts. In this bias-correction application, monthly precipitation values at 39 stations, which were obtained from the multi-GCM ensemble, were assessed for the reference period 1980–2005 under the historical scenario. Then, the probability plot correlation co-efficient test revealed that the two-parameter Gamma distribution fitted well at 39 stations. The CDFs pertaining to the observed data and the ensemble forecasts of four scenarios were computed. However, they are not presented due to page number restriction. The yield of the bias correction application in facilitating the distributional features of the forecasted precipitation values under the historical scenario to be convenient with those of observations at Akhisar station can be seen in Figure 6. The computed statistics of precipitation forecasts for the same example are given in Figure 6, also. Although the arithmetical mean, standard deviation, variation (C_v), median and maximum value statistics of the observed precipitation at Akhisar station are 46.45 mm, 52.43 mm, 1.129, 28.45 mm and 351.2 mm, respectively, those of precipitation forecasts for the historical scenario before correcting biases were 45.89 mm, 29.46 mm, 0.642, 41.98 mm and 124.17 mm, respectively. After correcting biases, these parameters under the historical scenario were 46.24 mm, 51.61 mm, 1.116, 31.37 mm and 309.6 mm, respectively. These results show that the biases were reduced meaningfully for the Akhisar station example. Similar inferences were found to be acceptable for the other 38 stations as well.

3.4. Hypothesis testing on historical scenario results

In order to have confidence in the climate change scenarios downscaled statistically from GCMs, assurance is required that the downscaled values can represent past climatic conditions closely (Dibike *et al.*, 2007). After bias correction, a method was employed in the study to analyse the confidence levels of both the downscaled results of the 12 GCMs and ensemble simulations derived from the BMA scheme, namely hypothesis testing based on the Mann–Whitney *U*-test, which was suggested by Dibike *et al.* (2007) also in uncertainty analyses of downscaled precipitation regimes. The formulations of this test were given by Okkan and Inan (2015a).

If the obtained asymptomatic significance values are greater than or equal to 5%, then there is no meaningful difference between observed and forecasted values in terms of the medians. As shown in Table 5 for Akhisar station, the Mann–Whitney

Table 5. Asymptomatic significance values derived from hypothesis testing for Akhisar station.

Climate model	Jan.	Feb.	Mar.	Apr.	May	Jun.	Jul.	Aug.	Sep.	Oct.	Nov.	Dec.
BCC-CSM1.1 (%)	38.97	21.33	36.98	0.75	18.16	27.22	24.52	35.54	1.65	0.27	59.56	19.38
CCSM4 (%)	38.97	18.76	100.00	66.05	16.43	0.06	8.37	33.66	95.62	34.13	39.99	95.62
CESM1(CAM5) (%)	16.99	82.62	25.65	2.81	2.56	0.01	44.76	66.05	98.54	74.18	19.38	63.42
Csiro-Mk3.6 (%)	2.32	9.22	52.18	8.21	11.55	53.38	64.73	6.19	25.65	3.86	85.48	74.18
GFDL-CM3 (%)	38.97	91.26	34.13	7.89	4.41	0.00	46.41	10.14	18.16	72.80	95.62	95.62
GFDL-ESM2M (%)	13.82	39.99	5.94	11.55	6.19	0.07	24.89	82.62	41.02	68.05	54.59	16.43
GISS-E2-H (%)	82.62	55.81	5.24	0.11	94.16	11.98	0.03	1.74	21.33	18.16	45.30	43.13
GISS-E2-R (%)	54.59	18.16	1.16	0.04	76.97	0.11	1.74	0.01	3.23	13.82	70.07	3.38
HADGEM2-ES (%)	62.12	52.18	67.38	15.34	4.61	0.04	0.12	64.73	70.07	3.95	5.70	79.78
IPSL-CM5A-LR (%)	36.98	20.67	79.78	0.27	74.18	0.00	0.00	64.73	7.89	31.86	0.41	71.43
MIROC-ESM (%)	42.07	86.92	21.33	12.42	16.43	13.34	16.71	16.99	24.15	66.71	62.12	5.70
MRI-CGCM3 (%)	13.34	0.51	6.72	10.34	2.01	0.03	0.08	46.97	24.15	0.01	95.62	31.41
ENSEMBLE (%)	91.26	86.92	92.71	85.48	85.48	74.18	25.65	9.95	36.02	98.54	92.71	84.05

The shaded characters in table displays that there is a significant difference between the observation and forecasted values for the median statistics.
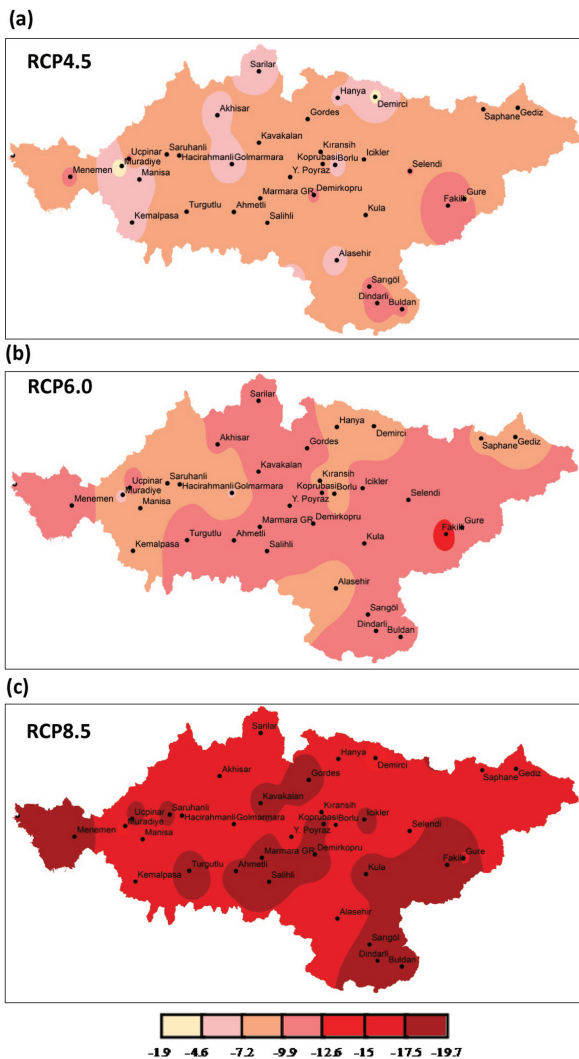

Figure 7. Precipitation changes (in %) in relation to the 1980–2005 historical scenario period for (a) RCP4.5, (b) RCP6.0 and (c) RCP8.5 scenarios.

U-test was implemented at the 5% level of significance to examine whether precipitation forecasts in the historical scenario were meaningfully different from observation statistics or not. According to analyses, it is interpreted that the corrected ensemble simulations are better than those of single GCMs. In other words, the combined use of the BMA-based ensemble procedure and bias correction approach was able to reproduce the median characteristics of monthly precipitation reasonably well. Similar results were obtained for the corrected ensemble simulations at the other 38 stations which were not presented here.

3.5. Foreseen changes in future precipitation

It is hoped that produced forecasts are not only reliable because multi-GCM ensemble application is more consistent than a single GCM usage, but also de-biased after the bias correction procedure. The distributions of precipitation changes are shown in Figure 7 for the considered future period (2015–2050) under three RCP scenarios. In the present study, in order to investigate whether the mean statistics related to produced forecasts under the three RCP scenarios reflecting the future period were statistically distinct from those of the historical scenario (1980–2005 climate), a two-sample t-test was operated at the 5% significance level.

The results in Figure 7 reveal that the precipitation over the basin tended to decrease in the future for all three RCP scenarios. However, remarkable decreases were found only in the RCP8.5 results, where the foreseen changes were statistically significant by t-test for nearly all stations. According to the RCP8.5 scenario, decreasing precipitation in the western part of the basin and some regions nearest to Golmarmara Lake and Demirkopru Dam and Gordes Dam reservoirs was more obvious than in the northwestern and northeastern parts of the Basin, whereas effective decreases also were found in the southeastern part of the basin, where the decreasing proportion was foreseen as 18.5%.

In order to interpret foreseen changes in precipitation over the whole basin, Thiessen weighted precipitation (TWP) values were obtained from all 39 stations. TWP obtained from the scenario forecasts for the 39 stations for both seasonal and annual periods are given (Figure 8). Although decreases were foreseen in all seasons under RCP8.5, it was much more distinctive in autumn. Moreover, the decreases foreseen in winter and autumn will affect annual precipitation regime because the total precipitation measured in winter and autumn represents nearly half of the total precipitation potential of the basin. When the annual mean statistics were considered, 8, 10 and 17% decreases were foreseen related to RCP4.5, RCP6.0, and RCP8.5 scenarios, respectively. Moreover, the box-plot graphs given in Figure 8 show that there will be decreases in the forecasts of third quartiles (high-rainfall), particularly in the RCP8.5 results. When the projected surface air temperature, which is expected
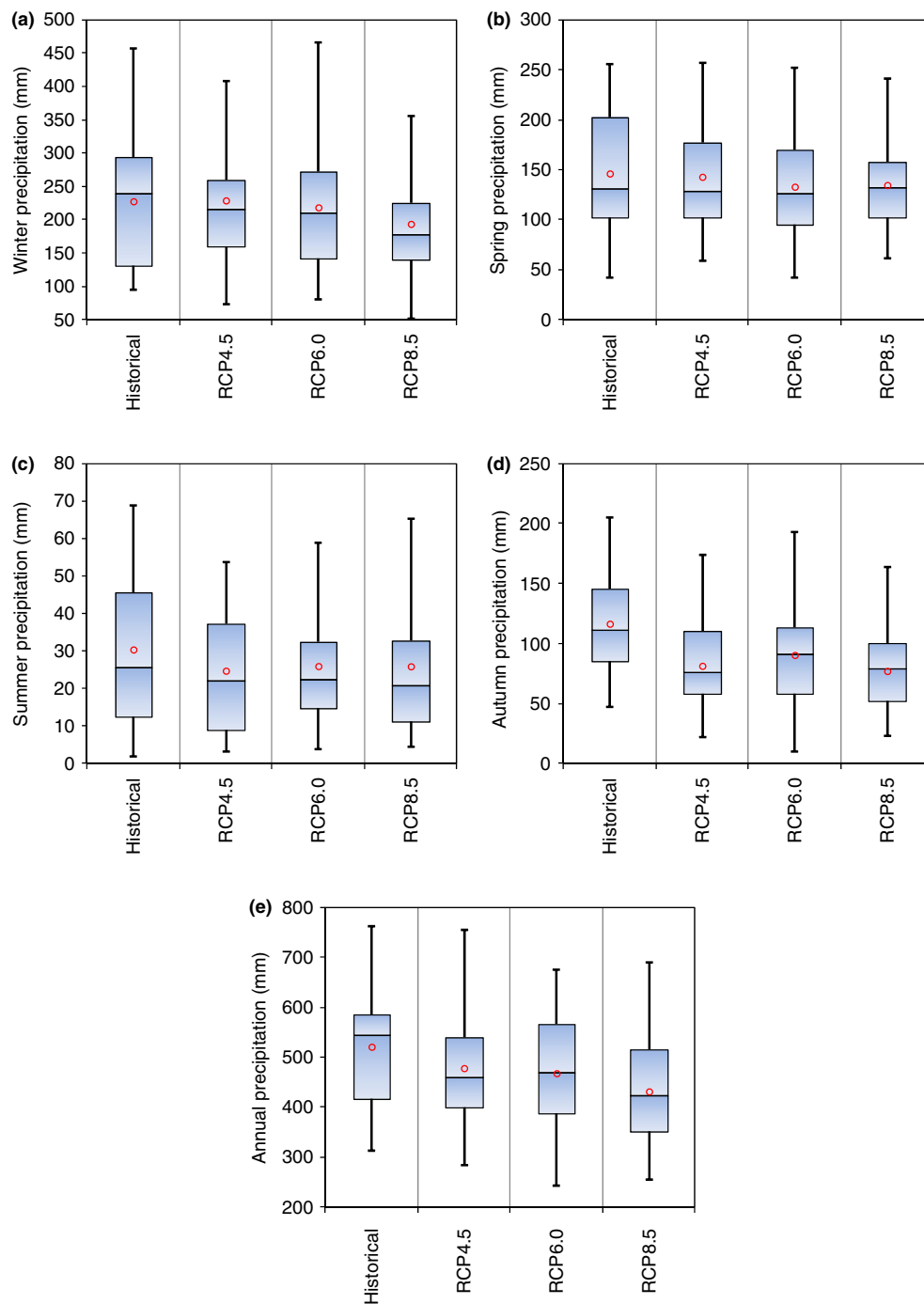
Figure 8. TWP calculated from the scenario forecasts of 39 stations for (a) winter, (b) spring, (c) summer, (d) autumn and (e) annual periods.

to increase markedly in all three RCP scenarios, is also taken into account, it becomes inevitable that the basin may experience water scarcity problem between the years 2015 and 2050.

4. Conclusions

The analysis of precipitation has a very important role to play in water resource management, such as planning of irrigation systems, dam reservoir operation, water budget studies and watershed modelling. In this study, projection of monthly precipitation over the Gediz Basin under several Representative Concentration Pathways (RCP) scenarios mentioned in the

IPCC 5th Assessment Report (AR5) was performed by a modelling strategy consisting of artificial neural network (ANN) / least-squares support vector machine (LSSVM) techniques, multi-general circulation model (GCM) ensemble and bias correction.

The statistical downscaling models were calibrated and tested using both observed precipitation and the ERA-Interim reanalysis predictor. The performance examination of the downscaled precipitation predictions at 39 stations denoted that the trained models generated consistent results, in contrast to various works in the literature where daily precipitation downscaling was carried out (e.g. Dibike et al., 2007). In other words, the good or very good agreement between observed and predicted monthly values

at meteorological stations indicated that the trained models with the set of optimized parameters could be applied to examine the responses of precipitation due to climate changes in the Basin.

Hence, the effectiveness of statistical downscaling models was illustrated through their integration to a historical scenario (1980–2005) and three RCP future scenarios (2015–2050). At this stage, simulations from 12 GCMs, which are available at CMIP5, were considered to obtain projections of precipitation at 39 stations. The eventual precipitation forecasts were produced from a multi-GCM ensemble application based on a Bayesian Model Averaging (BMA) method and bias correction technique. The quantile mapping based-bias correction (QM) approach employed in this study, which uses cumulative distribution functions (CDFs), especially for hydrological variables coming from a skewed distribution, was also preferred by other researchers. By using hypothesis testing, the ability of corrected ensemble forecasts to simulate the historical climate in terms of statistical moments was assessed. Sachindra et al. (2014) have emphasized that quantile mapping is not able to correct the time series explicitly. Otherwise, methods such as monthly bias-correction and nested bias-correction are able to correct some of the statistics without disrupting the temporal sequence (Sachindra et al., 2014). Therefore, the QM approach presented herein will be compared with other bias correction methods in a future work in order to ensure the validation of the results derived from this study.

Following the investigation of historical scenario results, the significances of the computed changes for the 2015–2050 future period were examined statistically. According to statistical investigations for different emission scenarios, insignificant decreases are foreseen over the Basin for RCP4.5 and RCP6.0, whereas significant decreasing trends in precipitation are identified for the RCP8.5 scenario. Considering that the RCP8.5 scenario results can be defined as a pessimistic scenario with comparatively high greenhouse gas emissions, it is foreseen that there will be around 17% decrease in mean areal precipitation over the basin compared to the reference climate period.

As is well-known, in downscaling works the possible effects of climatic change on variables operating within the hydrological cycle are all related within the uncertainty/reliability frame. It was uttered that uncertainties are related to GCMs, used scenarios, data features, and the used downscaling techniques (Mujumdar and Ghosh, 2008; Okkan and Inan, 2015a). In spite of the aforementioned uncertainties, statistical downscaling techniques will remain the most frequently used tools for researchers to examine the effects of climate change on hydrological processes owing to their computational practicality compared to dynamic downscaling (Anandhi et al., 2008). Moreover, the use of 12 GCMs with 3 RCP scenarios, two statistical downscaling models trained with optimal predictor selection and an ensemble procedure should serve as inspiration for precipitation projections of other important basins in Turkey and beyond.

Duan et al. (2007) stated that different models may have strengths in capturing different aspects of hydro-meteorological processes. Enough knowledge about the uncertainty relevant to the forecasts derived from single models currently may not be available. However, the uncertainties and structural errors observed in any single model are at insignificant orders for ensemble applications. In this regard, focusing on both Bayesian model averaging and bias correction methods for this study resulted in robust climate modelling and a reliable projection.

The inferences obtained from this work point out that the developed strategy is a conceivable option for downscaling precipitation to a basin scale. Hence, a similar study concerning surface air temperature projection for the same basin will be performed in a future study. However, it is proposed that dynamical downscaling tools (e.g. REGCM4, PRECIS) and other statistical models used in the literature can be used to check for inter-model robustness of the downscaled forecasts for the study area. A comprehensive research effort in this direction is also planned.

The results presented herein will also be assessed in future work through the integration of rainfall–runoff models. Following building a rainfall–runoff model for the sub-basins in the Basin, the downscaled precipitation and temperature values can be converted into streamflows by operating a calibrated hydrological model.

Acknowledgements

References

Anandhi A, Srinivas VV, Nanjundiah RS, Nagesh Kumar D. 2008. Downscaling precipitation to river basin in India for IPCC SRES scenarios using support vector machine. *Int. J. Climatol.* **28**: 401–420.

Bürger G, Murdock TQ, Werner AT, Sobie SR, Cannon AJ. 2012. Downscaling extremes-an intercomparison of multiple statistical methods for present climate. *J. Clim.* **25**: 4366–4388.

Chen H, Guo J, Xiong W, Guo S, Xu C-Y. 2010. Downscaling GCMs using the Smooth Support Vector Machine method to predict daily precipitation in the Hanjiang Basin. *Adv. Atmos. Sci.* **27**: 274–284.

Chong-hai X, Ying X. 2012. The projection of temperature and precipitation over China under RCP Scenarios using a CMIP5 multi-model ensemble. *Atmos. Ocean. Sci. Lett.* **5**: 527–533.

Dibike YB, Gachon P, St-Hilaire A, Ouarda TBMJ, Nguyen VTV. 2007. Uncertainty analysis of statistically downscaled temperature and precipitation regimes in Northern Canada. *Theor. Appl. Climatol.* **91**: 149–170.

Duan Q, Ajami N, Gao X, Sorooshian S. 2007. Multi-model ensemble hydrologic prediction using Bayesian model averaging. *Adv. Water Resour.* **30**: 1371–1386.

Fistikoglu O, Okkan U. 2011. Statistical downscaling of monthly precipitation using NCEP/NCAR reanalysis data for tahtali river basin in Turkey. *J. Hydrol. Eng.* **16**: 157–164.

Fowler HJ, Blenkinsop S, Tebaldi C. 2007. Linking climate change modelling to impacts studies: recent advances in downscaling techniques for hydrological modelling. *Int. J. Climatol.* **27**: 1547–1578.

Ghosh S, Mujumdar PP. 2008. Statistical downscaling of GCM simulations to streamflow using relevance vector machine. *Adv. Water Resour.* **31**: 132–146.

Gleckler P, Taylor K, Doutriaux C. 2008. Performance metrics for climate models. *J. Geophys. Res.* **113**: D06104.

Goyal MK, Ojha CSP. 2012. Downscaling of surface temperature for lake catchment in an arid region in India using linear multiple regression and neural networks. *Int. J. Climatol.* **32**: 552–566.

Haas R, Pinto JG. 2012. A combined statistical and dynamical approach for downscaling large-scale footprints of European windstorms. *Geophys. Res. Lett.* **39**: L23804.

Hagan MT, Menhaj MB. 1994. Training feedforward networks with the Marquardt algorithm. *IEEE. Trans. Neural. Netw.* **5**: 989–993.

Hessami M, Gachon P, Ouarda TBMJ, St-Hilaire A. 2008. Automated regression-based statistical downscaling tool. *Environ. Modell. Softw.* **23**: 813–834.

Ines AVM, Hansen JW. 2006. Bias correction of daily GCM rainfall for crop simulation studies. *Agric. For. Meteorol.* **138**: 44–53.

Ji Z, Kang S. 2013. Double-nested dynamical downscaling experiments over the Tibetan Plateau and Their Projection of climate change under Two RCP Scenarios. *J. Atmos. Sci.* **70**: 1278–1290.

Kim J, Choi J, Choi C, Park S. 2013. Impacts of changes in climate and land use/land cover under IPCC RCP scenarios on streamflow in the Hoeya River Basin. *Korea. Sci. Total. Environ.* **452–453**: 181–195.

Knutti R, Abramowitz G, Collins M, Eyring V, Gleckler PJ, Hewitson B et al. 2010. Good practice guidance paper on assessing and combining multi model climate projections. *IPCC Expert Meeting on Assessing and Combining Multi Model Climate Projections*: Boulder, CO; 15pp.

Lafon T, Dadson S, Buys G, Prudhomme C. 2013. Bias correction of daily precipitation simulated by a regional climate model: a comparison of methods. *Int. J. Climatol.* **33**: 1367–1381.

Lee JW, Hong SY, Chang EC, Suh MS, Kang HS. 2014. Assessment of future climate change over East Asia due to the RCP scenarios downscaled by GRIMs-RMP. *Clim. Dyn.* **42**: 733–747.

Leung LR, Mearns LO, Giorgi F, Wilby RL. 2003. Regional climate research: needs and opportunities. *Bull. Am. Meteorol. Soc.* **84**: 89–95.

Meinshausen M, Smith SJ, Calvin K, Daniel JS, Kainuma MLT, Lamarque J, *et al*. 2011. The RCP greenhouse gas concentrations and their extensions from 1765 to 2300. *Clim. Change* **109**: 213–241.

Moriasi DN, Arnold JG, Van Liew MW, Bingner RL, Harmel RD, Veith TL. 2007. Model evaluation guidelines for systematic quantification of accuraccy in watershed simulations. *Trans. Asabe.* **50**: 885–900.

Moss RH, Edmonds JA, Hibbard KA, Manning MR, Rose SK, van Vuuren DP, *et al*. 2010. The next generation of scenarios for climate change research and assessment. *Nature* **463**: 747–756.

Mujumdar PP, Ghosh S. 2008. Modeling GCM and scenario uncertainty using a possibilistic approach: application to the Mahanadi River. *India. Water. Resour. Res.* **44**: W06407, DOI: 10.1029/2007WR006137.

Okkan U. 2015. Assessing the effects of climate change on monthly precipitation: proposing of a downscaling strategy through a case study in Turkey. *KSCE J. Civ. Eng.* **19**: 1150–1156.

Okkan U, Fistikoglu O. 2014. Evaluating climate change effects on runoff by statistical downscaling and hydrological model GR2M. *Theor. Appl. Climatol.* **117**: 343–361.

Okkan U, Inan G. 2015a. Statistical downscaling of monthly reservoir inflows for Kemer watershed in Turkey: use of machine learning methods , multiple GCMs and emission scenarios. *Int. J. Climatol.* **35**: 3274–3295.

Okkan U, Inan G. 2015b. Bayesian learning and relevance vector machines approach for downscaling of monthly precipitation. *J. Hydrol. Eng.* **20**, DOI: 10.1061/(ASCE)HE.1943-5584.0001024.

Raftery AE, Gneiting T, Balabdaoui F, Polakowski M. 2005. Using bayesian model averaging to calibrate forecast ensembles. *Mon. Weather Rev.* **133**: 1155–1174.

Riahi K, Rao S, Krey V, Cho C, Chirkov V, Fischer G, *et al*. 2011. RCP 8.5-A scenario of comparatively high greenhouse gas emissions. *Clim. Change.* **109**: 33–57.

Sachindra DA, Huang F, Barton A, Perera BJC. 2013. Least square support vector and multi-linear regression for statistically downscaling general circulation model outputs to catchment streamflows. *Int. J. Climatol.* **1106**: 1087–1106.

Sachindra DA, Huang F, Barton A, Perera BJC. 2014. Statistical downscaling of general circulation model outputs to precipitation-part 2: bias-correction and future projections. *Int. J. Climatol.* **34**: 3282–3303.

Salathé EP. 2003. Comparison of various precipitation downscaling methods for the simulation of streamflow in a rainshadow river basin. *Int. J. Climatol.* **23**: 887–901.

Schmidli J, Frei C, Vidale PL. 2006. Downscaling from GCM precipitation: a benchmark for dynamical and statistical downscaling methods. *Int. J. Climatol.* **26**: 679–689.

Semenov MA. 2008. Simulation of extreme weather events by a stochastic weather generator. *Clim. Res.* **35**: 203–212.

Singh V, Goyal MK. 2016. Analysis and trends of precipitation lapse rate and extreme indices over north Sikkim eastern Himalayas under CMIP5ESM-2 M RCPs experiments. *Atmos. Res.* **167**: 34–60.

Suykens JAK. 2001. Nonlinear modelling and support vector machines. *IMTC 2001. Proceedings of the 18th IEEE Instrumentation Measurement Technology Conference Rediscovering Measurement in the Age of Informatics (Cat. No.01CH 37188)*, 21–23 May 2001, Budapest, Hungary.

Tatli H, Dalfes N, Menteş S. 2004. A statistical downscaling method for monthly total precipitation over Turkey. *Int. J. Climatol.* **24**: 161–180.

Themeßl M, Gobiet A, Leuprecht A. 2011. Empirical-statistical downscaling and error correction of daily precipitation from regional climate models. *Int. J. Climatol.* **31**: 1530–1544.

Tripathi S, Srinivas VV, Nanjundiah RS. 2006. Downscaling of precipitation for climate change scenarios: a support vector machine approach. *J. Hydrol.* **330**: 621–640.

Vu MT, Aribarg T, Supratid S, Raghavan SV, Liong S-Y. 2015. Statistical downscaling rainfall using artificial neural network: significantly wetter Bangkok? *Theor. Appl. Climatol.*, DOI: 10.1007/s00704-015-1580-1.

Wilby R, Dawson C, Barrow E. 2002. A decision support tool for the assessment of regional climate change impacts. *Environ. Model. Softw.* **17**: 145–157.

Wilby RL, Hassan H, Hanaki K. 1998. Statistical downscaling of hydrometeorological variables using general circulation model output. *J. Hydrol.* **205**: 1–19.

Wilby RL, Wigley TML. 1997. Downscaling general circulation model output: a review of methods and limitations. *Prog. Phys. Geogr.* **21**: 530–548.

Xoplaki E, González-Rouco JF, Luterbacher J, Wanner H. 2004. Wet season Mediterranean precipitation variability: influence of large-scale dynamics and trends. *Clim. Dyn.* **23**: 63–78.